Chapter 3

Single gold nanowire utilized RI SPR optical fiber sensor

In this chapter, I design and numerically simulate a single Au-nanowire (S-AuNW) assisted inside the hole in the fiber cladding structure based highly sensitive refractive index (RI) sensing surface plasmon resonance (SPR) sensor. By measuring the resonant peaks shift, I have obtained the variation in the analyte RIs. my designed sensor model has achieved significant sensitivity, with an average wavelength sensitivity of 6700 nm/RIU and a maximum sensitivity of 14000 nm/RIU. Furthermore, the sensor obtained a high resolution and the highest figure of merit (FOM) value of 7.14 × 10^{-6} RIU and 124.54 RIU^{-1}, respectively, within the analyte RI range of 1.33-1.43. By placing the analyte inside the hole, it is shielded from the surrounding environment, making the sensor more robust and suitable for detecting toxic or environmentally affected gases and chemicals.

3.1 Introduction

The incident light confined evanescently to the surface of plasmonic material and induced the collective oscillations of the conduction-free electrons, known as surface plasmons[119]. The surface plasmon wave (SPW) is excited along a plasmonic material-dielectric interface by continuous oscillations of surface plasmons, and these oscillations are more sensitive to changes in the external medium RI[120 93]. Surface plasmon resonance (SPR) occurs due to the coupling between the propagation vector of an evanescent wave of incident light and SPW, resulting in the transfer of the maximum energy of incident light to the metal conduction electrons. The specific resonance wavelength (λ_{res}) is achieved when incident light energy and conduction electrons in plasmonic material are perfectly coupled or phase-matched[121]. The resonance wavelength (λ_{res}) of each SPR condition is highly sensitive to external perturbations in the surrounding medium. This property is utilized in SPR-based sensors as a sensing mechanism. Surface plasmon resonance is a widely employed surface-sensing analytical technique that is used for sensing applications such as physical parameter sensing, biosensing, food quality recognition, gas detection, chemical sample, and detection environmental condition screening due to its high sensitivity[122 123]. The combination of optical fiber technology and the SPR sensing methodology has been extensively researched and applied across multiple disciplines due to its simple structure, small size, low-cost fabrication, high accuracy, maximum sensitivity, remote sensing capability, and real-time detection without labelling. Enhanced versatility and integration potential are provided by miniaturized fiber SPR sensors[124].

Various structure shapes of SPR-based optical fiber sensors have been designed and analyzed for measuring refractive index (RI), relative humidity (RH), Strain, and temperature, such as microstructure optical fiber, conventional/unconventional multimode optical fiber, and single-mode optical fiber[125 126 127 128]. Traditional optical fiber sensors are

simpler to fabricate and less expensive compared to microstructured optical fiber SPR sensors. Traditionally, plasmon-activated materials such as gold (Au), indium tin oxide (ITO), copper (Cu), silver (Ag), and Al-doped ZnO (AZO) are used in plasmonic-based sensors due to their active absorption properties[77] [129]. For SPR conditions, researchers use the thin films and nanoparticles (nanowires, nanorods, etc.) type's configurations in the sensor devices. In last years, many thin films using plasmonic-based optical fiber sensor papers are published in different journals. For example, in 2014 S. Shukla et al. proposed the RI detection bi-layers of the metal-ZnO plasmonic-based optical fiber sensor. The ZnO layer is coated over the metallic layer to enhance the sensitivity and the sensor obtained the maximum sensitivity of 3161 nm/RIU for bilayers of 40 nm Au / 15 nm ZnO. Good performance refractive index sensing SPR fiber sensor had been suggested by R. Nasirifar et al. in which silver (Ag) and Gold (Au) thin films coated double channel are used for the detection of the analytes The sensor displayed sensitivities of 1200 nm/RIU and 1650 nm/RIU for its first and second channels, respectively, and had average FOM values of 46 RIU^{-1} and 55 RIU^{-1} [130]. An SPR-based D-shaped RIs sensing fiber sensor had been designed by S. K. Dubey et al. in 2022. The given sensor demonstrated the highest sensitivities of 9810 nm/RIU and 15310 nm/RIU for Ag/SnO_2 and Ag/TiO_2 grating structures respectively[131]. S. K. Mishra et al. investigated the bi-layer ITO/polymer-coated SPR-based RI optic fiber sensor in 2021. The use of ITO as the plasmonic material, combined with a polymer, enhances the performance of the sensor. For analytes RIs range 1.33 -1.38, the sensing probe exhibits maximum values of FOM, DA, and sensitivity, which are respectively 22.07 1/RIU, 2.62 μm^{-1}, and 10.28 μm/RIU[132]. It has been observed that plasmonic sensors based on nanofilm structures are complex, which can hinder achieving maximum sensitivity and higher FOM.

To overcome issues with thin film coatings, researchers have developed metallic nanowire or nanorod-used fiber sensors for both internal and external sensing applications. For example, in 2015 D. Feng et al. had been designed an infrared RI SPR sensor using bi-metallic nanowire grating. This sensor detected the RI of the analyte range of 1.33-1.49 and achieved the highest sensitivity of 643.75 nm/RIU[17]. In 2017, D. F. Santos et al. investigated an Au-wire-assisted D-type fiber SPR sensor. By employing the wavelength interrogation method, numerical analysis was conducted to evaluate the resolution and sensitivity for different RI of the analyte range 1.30 - 1.40. The sensor achieved the optimum sensitivity of 8437 nm/RIU[53]. For low RI analytes detection, a hollow-core metal nanowire-assisted SPR sensor had been reported by A. K. Pathak et al. in 2019. Through analysis of the results, a maximum sensitivity of 12400 nm/RIU was achieved for Cu nanowire with a resolution of 1.6×10^{-6} RIU[56]. In 2020, R. A. Kadhim investigated an SPR-based refractive index (RI) biosensor that used many D-shaped Ag nanowires. Through simulation analyses, it was found that the sensor's maximum sensitivity of 5100 nm/RIU for surrounding RIs range of 1.35-1.39. The nanowire grating-assisted D-shaped fiber SPR sensor had been proposed by Q. Ren et al. in 2022. The sensor was capable of detecting analyte refractive indices (RI) in the range of 1.31 to 1.37[133]. Many previously proposed fiber sensors have demonstrated good performance for RIs sensing, but challenges such as complicated fabrication processes, sensing of toxic liquid chemicals and gases, and the detection of highly environmentally reactive analytes still persist.

My main purpose is to investigate a simple structure SPR fiber that can be easily designed and capable of detecting highly environmentally reactive analytes with maximum sensitivity by introducing a single Au nanowire used inside a hole in the fiber cladding. The sensing condition occurs at the interface between the nanowire and the analyte, which happens when

the analyte is placed inside the hole. To simulate and analyze the modes, I have utilized COMSOL Multiphysics software to optimize separation between the hole and core boundary(B_s), the diameter of the hole (D_h), and the diameter of the Au-nanowire (d_{Au}) based on the finite element method (FEM). At the optimized sensor parameters of B_s = 0.10 μm, D_h = 25 μm, and d_{Au} = 500 nm, I have calculated the sensor performance parameters wavelength sensitivity, FOM, and resolution. My designed sensor is capable of detecting toxic and environmentally reactive liquid chemicals and gases as well. This is because the analytes, which are filled inside the hole, are covered with the fiber cladding material in my sensor.

3.2 Sensor structure modeling

A schematic cross-section view of an SPR RI sensor based on a structure with an S-AuNW assisted inside the hole in the fiber cladding region is illustrated in Fig. 3.1. Inside the hole in the fiber cladding region, both the S-AuNW and analyte are placed. In my research, an optical fiber with a 125 μm cladding diameter and an 8.4 μm core diameter is used. The hole inside the fiber cladding region designed structure sensor can be fabricated using various techniques such as micro-drilling Q-switched Nd: YAG laser technique, electron beam micromachining, and other high-power laser irradiation techniques. The S-AuNW can be easily placed inside the hole in the fiber cladding region using templated synthesis and lithography techniques[134 135]. In my work, I represent the separation between the hole and core boundary, the diameter of the hole, and the diameter of the S-AuNW by the B_s, D_h, andd_{Au}, respectively.

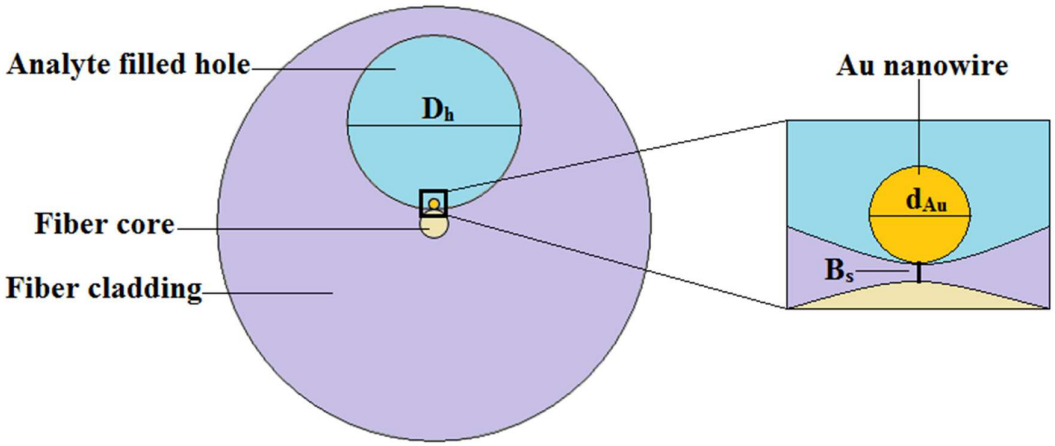

Fig. 3.1 The designed structural model cross-section view.

In my work, the cladding and core of the SMF used are made of fluorine (F)-doped fused silica and germanium (Ge)-doped fused silica, respectively. The refractive indices of these materials are calculated using the Sellmeier relation, which is defined as [102 75]

$$n(\lambda) = Sqrt\left(1 + \frac{g_1\lambda^2}{\lambda^2 - h_1^2} + \frac{g_2\lambda^2}{\lambda^2 - h_2^2} + \frac{g_3\lambda^2}{\lambda^2 - h_3^2}\right) \quad (3.1)$$

The Sellmeier coefficients (g_1, g_2, g_3 and h_1, h_2, h_3) for cladding and core of the fiber are given in Table 3.1.

Table 3.1 The fiber's cladding and core's Sellmeier coefficients.

Coefficients	g_1	g_2	g_3	h_1 (µm)	h_2 (µm)	h_3 (µm)
Cladding (F-doped silica)	0.696166	0.407942	0.897479	0.068404	0.116241	9.89616
Core (Ge-doped silica)	0.6867	0.4348	0.8966	0.07268	0.1151	10.00

Equation 3.2 uses the Drude model to calculate the wavelength-dependent dielectric constant of gold (Au) nanowires[103]

$$\varepsilon_{Au}(\lambda) = \varepsilon_{Re}(\lambda) + j\varepsilon_{Im}(\lambda) = 1 + \frac{\lambda^2 \lambda_{cw}}{\lambda_{pw}^2(\lambda_{cw} + j\lambda)} \tag{3.2}$$

The plasma and collision wavelengths of the plasmonic gold (Au) nanowire are denoted by λ_{pw} and λ_{cw} respectively, with values of 0.16826 µm and 8.9342 µm

3.3 Numerical Result and Discussion

For every SPR-based fiber sensor, the key parameter is the confinement loss (CL) of the core-guided mode, which is calculated to characterize the SPR sensing scheme. The CL of the core-guided mode can be affected by the analyte's refractive index, and it is used to determine the resonance wavelength (λ_{res}) and RI detection range of the proposed SPR sensor. The effective RI imaginary part $Im(n_{eff})$ dependent CL (α_{CL}) of the designed sensor is measured by equation 3.3 [76].

$$\alpha_{CL} = \frac{Im(n_{eff})}{\lambda} \times 54.5757 \times 10^4 \left[\frac{dB}{cm}\right] \tag{3.3}$$

Where λ (in µm) represents the source wavelength.

Fig. 3.2 insets (a)-(c) represents the electric field (EF) intensity distribution in the fundamental core guided, SPW, and coupling mode, respectively. The black and blue plots show the effective index real values and confinement loss values, respectively at analyte RI = 1.37, for the optimized parameters of my designed structure, which are B_s = 0.10 µm, D_h = 25 µm, and d_{Au} = 0.25 µm. The effective index real values decrease continuously with increasing wavelengths. However, the CL values initially increase and then decrease continuously after the perfect resonance peak. The core-guided mode maximum energy transfers to the SPW mode due to coupling between the core-guided and SPW mode, resulting in a loss peak find in the loss spectra at an 850 nm specific wavelength. This specific wavelength is referred to as the resonance wavelength (λ_{res}).

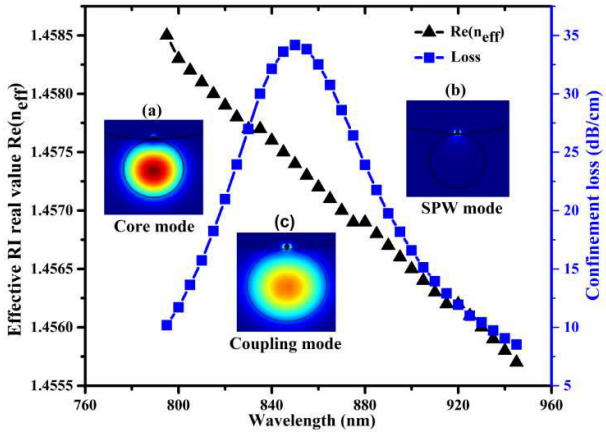

Fig. 3.2 Electric field distribution in the modes and effective RI real values and loss values spectra at analyte RI = 1.37.

In the simulations, the incident light is assumed to propagate along the Z-direction; this means that all the modes analysis is performed in the XY plane. The separation between the hole and core curve boundary, represented as B_s, is an affected parameter in determining the sensing results of the designed sensor. The evanescent wave generated by the core mode of the fiber must be strong enough to excite the surface plasmons on the S-AuNW surface, which then interacts with the surrounding analyte, leading to a shift in the λ_{res} in the CL

spectra. Fig. 3.3(a) shows the variation of CL with respect to the wavelength at analyte RI 1.35 for different values of curve boundary separation (B_s) ranging from 0.10 to 0.30 μm. when curve boundary separation is increased (B_s = 0.10, 0.20, and 0.30 μm), the CLs are 21.23, 18.20, and 15.19 dB/cm, respectively. It is clear that the CL decreases with increasing curve boundary separation (B_s) and the maximum CL value is achieved for B_s = 0.10 μm at 765 nm wavelength. A larger separation between the hole and core curve boundary would result in a weaker evanescent wave and lower coupling efficiency between the SPW and core mode, leading to reduced sensor sensitivity. Conversely, a smaller separation would lead to increased coupling efficiency but may also result in higher losses due to the higher overlapping between the core and SPW mode. Therefore, the optimal value of B_s (= 0.10 μm) needs to be determined through simulation and optimization.

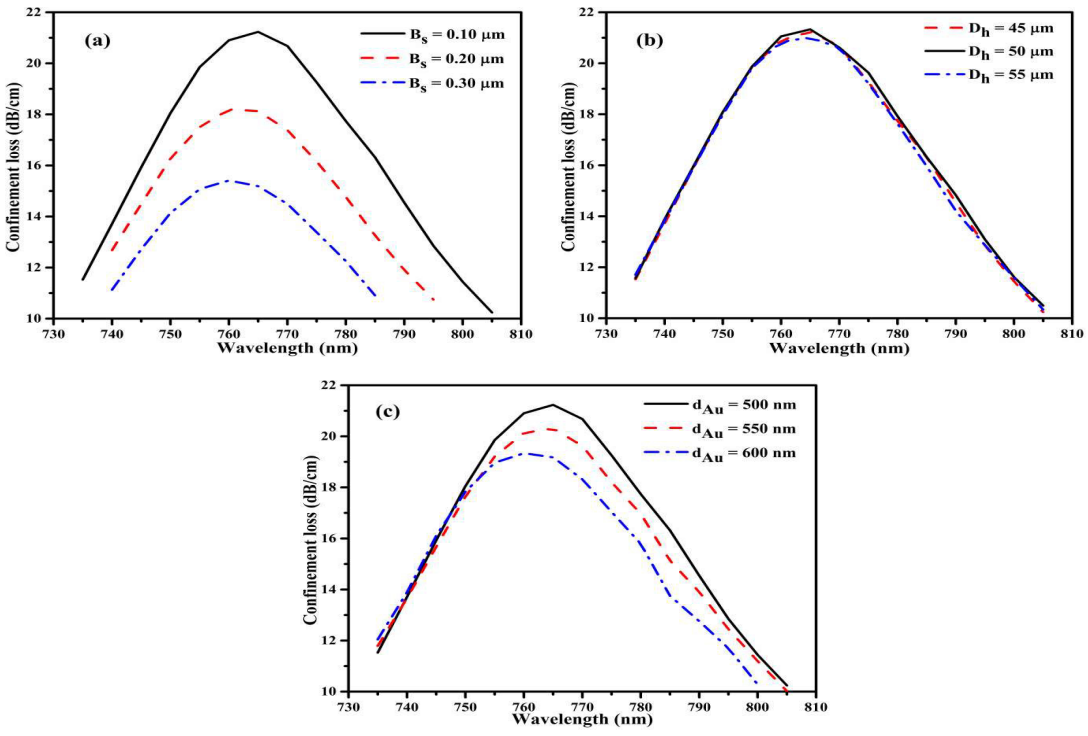

Fig. 3.3 Variation in loss spectra of the designed model at different **(a)** separations (B_s) **(b)** hole diameter (D_h) **(c)** S-AuNW diameter (d_{Au}).

The diameter of the hole (D_h) also affects the SPR condition of the investigated design structure, as both the analyte and S-AuNW are placed inside the hole region. In Fig. 3.3(b), the relationship between the CL values and incident light wavelength is illustrated for different hole diameters (D_h) while keeping B_s = 0.10 µm and d_{Au} = 500 nm fixed. The CL values of the designed sensor at RI of 1.35 with hole diameters of 45 µm, 50 µm, and 55 µm are 21.23 dB/cm, 21.33 dB/cm, and 21.01 dB/cm, respectively. I have taken D_h = 50 µm as the optimized parameter for my structure since the CL peak value is maximum at this value. The diameter of the S-AuNW (d_{Au}) can significantly affect the SPR condition and results performance of the proposed sensor. By optimizing the diameter of the S-AuNW, I can achieve the strongest SPR and improve the sensing performance results. The impact of the S-AuNW diameter (d_{Au}) variation on the CL spectra at an analyte RI of 1.35, and a fixed B_s of 0.10 µm and D_h of 50 µm, is illustrated in Fig. 3.3(c). As the diameter of S-AuNW increases from 500 nm to 600 nm, the resonance wavelengths exhibit a blue shift, and the CL peaks gradually decrease. The evanescent field can generate the SPW more easily when the S-AuNW diameter is small. As observed, the smallest S-AuNW diameter produces the highest CL peak. Therefore, d_{Au} = 500 nm is chosen as the optimized value.

Introducing an analyte with a different RI into the sensing region results in a shift in the λ_{res} in the CL spectra of the sensor. This wavelength shift can be detected by measuring the change in the CL peaks. As a result, the sensor is highly versatile and can be applied in diverse fields. Figs. 3.4(a) and 3.4(b) show variation in the CL values with the wavelengths for analyte RIs range of 1.33 -1.43. The CL peak values increase and shift towards longer wavelengths as the analyte RIs increase. Different analytes' RIs exhibit different propagation constants which affect the sensor's coupling behaviors. The full-width at half maximum (FWHM) of the CL peak broadens as the RIs increase. This broadening is due to the relatively lower index contrast caused by the increase in the RI of the analyte.

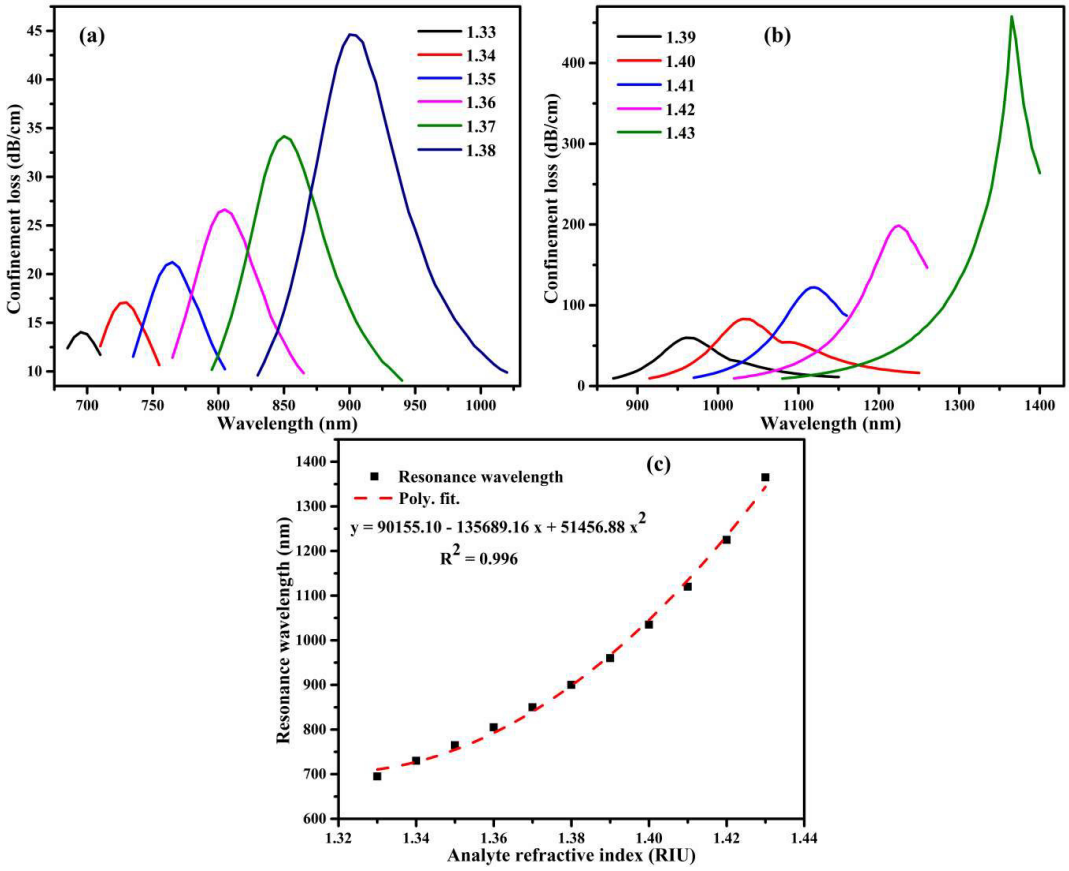

Fig. 3.4 (a-b) Loss spectra for different RIs (c) variations in resonance wavelength with RIs.

The designed sensor exhibits a good performance with a linear response, allowing for proper calibration and high accuracy. The highest peak values in the CL spectra correspond to the wavelength at which the SPR occurs and are therefore considered to be the resonance wavelength for different analytes RIs. Fig. 3.4(c) indicates the resonance wavelength polynomial fitting relationship with the RIs of the analyte, which confirms the high sensitivity of the designed sensor. The resonance wavelength polynomial regression equation as a function of RI is also shown in Fig. 3.4(c) with the coefficient of determination (R^2).

The Sensitivity, FWHM, resolution, and figure of merit (FOM) are the effective performance parameters for analyzing the sensor results. The proposed sensor performance parameter wavelength sensitivity (S_λ) can be determined by the following relation[56]

$$S_\lambda(nm/RIU) = \frac{\Delta\lambda_{res}}{\Delta RI} \tag{3.4}$$

Where $\Delta\lambda_{res}$ expresses the resonance wavelength change and ΔRI shows the analyte RI change. The performance parameter FOM of the designed sensor can be obtained by the following relation (3.5)[54]

$$FOM(RIU^{-1}) = \frac{S_w}{FWHM} \tag{3.5}$$

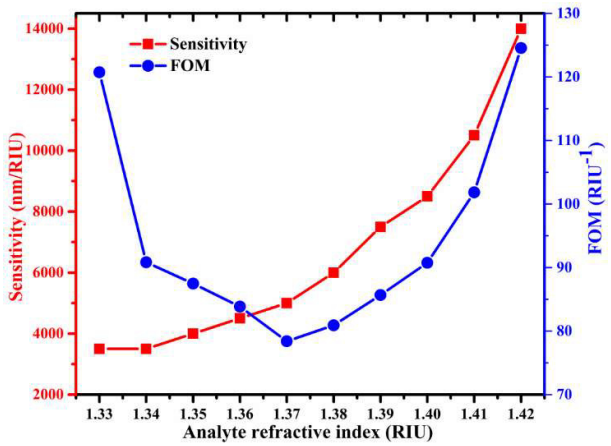

Fig. 3.5 Variations in the sensitivity and FOM with the RIs.

The sensor sensitivity expresses the wavelength shift with respect to a small change in analyte RI. The sensitivity and FWHM of the resonance peak are also factors included in the FOM, which is a sensor performance parameter. In Fig. 3.5, the sensitivity and corresponding FOM variation with the analyte RIs have presented. The sensitivity values increase as the RIs increase, which means that my sensor is more responsive to changes in the higher RIs of the analyte. The designed sensor has achieved the highest FOM of 124.54 RIU^{-1} for analyte RIs ranging from 1.42 to 1.43. Equation (3.6) is used to determine the sensor's resolution[136]

Table 3.2 Proposed sensor performance results at the optimized parameters.

Analyte RI	Res. Wav. (nm)	Conf. loss (dB/cm)	Res. peak shift (nm)	FWHM (nm)	Sen. (nm/RIU)	FOM (RIU^{-1})	Resolution (RIU)
1.33	695	14.04	35	28.99	3500	120.73	2.857×10^{-5}
1.34	730	17.09	35	38.53	3500	90.83	2.857×10^{-5}
1.35	765	21.23	40	45.72	4000	87.48	2.50×10^{-5}
1.36	805	26.63	45	53.66	4500	83.86	2.222×10^{-5}
1.37	850	34.17	50	63.77	5000	78.40	2.000×10^{-5}
1.38	900	44.62	60	74.17	6000	80.90	1.667×10^{-5}
1.39	960	59.81	75	87.55	7500	85.67	1.333×10^{-5}
1.40	1035	83.54	85	93.66	8500	90.75	1.176×10^{-5}
1.41	1120	122.17	105	103.10	10500	101.84	9.520×10^{-6}
1.42	1225	198.71	140	112.41	14000	124.54	7.140×10^{-6}
1.43	1365	457.76	-	99.53	-	-	-

Table 3.3 Comparison with other nanowire-assisted SPR sensors.

Reference	Type of nanowire	Analyte RI	Maximum Sensitivity (nm/RIU)	FOM (RIU^{-1})	Resolution (RIU)
56	Cu NW	1.46-1.48	12400	-	1.61×10^{-6}
54	Graphene coated Ag-NW	1.33-1.39	8860.93	70	-
137	Ag NW	1.33-1.38	9314.28	-	1.073×10^{-5}
138	AgNWs	1.35-1.39	5100	-	-
139	AuNW	1.33-1.41	12974	-	7.71×10^{-6}
140	Au/F3O4 NW	1.33-1.39	8500	-	1.17×10^{-6}
Proposed sensor	Single AuNW	1.33-1.43	14000	124.54	7.14×10^{-6}

$$R = \frac{\Delta RI \times \Delta\lambda_{min}}{\Delta\lambda_{res}} \ (RIU) \tag{3.6}$$

Where $\Delta\lambda_{res}$ and ΔRI represent the resonance wavelength shift and analyte RI change. Assuming a minimum spectral resolution of $\Delta\lambda_{min} = 0.1\,nm$, my proposed sensor has achieved a good resolution of 7.14×10^{-6} RIU, indicating its capability to measure small variations in analyte RI.

Fabrication errors during the manufacturing process can have a significant effect on the sensor results. It is important to consider these potential errors and to minimize their impact on the device's performance[141]. The manufacturing errors in the separation between

the core and hole curve boundary (B_s), the diameter of the hole (D_h), and the diameter of the S-AuNW (d_{Au}) can affect the sensor results performance. These structure parameters should be carefully controlled during the experimental fabrication process to minimize any errors and ensure high sensor performance.

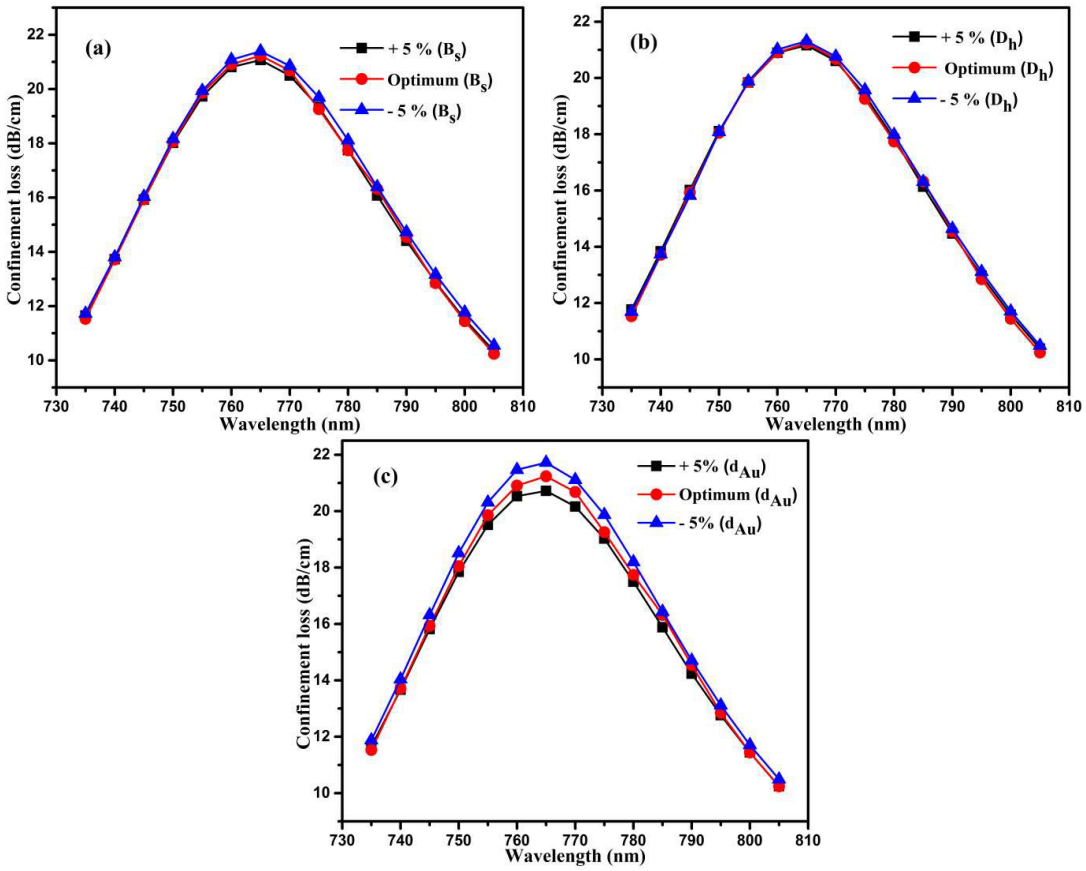

Fig. 3.6 Variations in the CL spectra for ± 5 % change in optimum value **(a)** separation ($\boldsymbol{B_s}$) **(b)** hole diameter ($\boldsymbol{D_h}$) **(c)** S-AuNW diameter($\boldsymbol{d_{Au}}$).

Figs. 3.6(a-c) represent the loss spectra for B_s, D_h, and d_{Au}, respectively, with a ± 5% variation at an RI value of 1.35. The simulations showed that the variation in the loss spectra was due to ± 5% variation in the fabrication parameters (B_s, D_h, and d_{Au}) have negligible, indicating that the sensor's performance is robust against ± 5% small fabrication errors. This is a promising finding as it suggests that the sensor can maintain its high sensitivity and accuracy even in practical manufacturing conditions. Due to its high sensitivity, resolution,

and accuracy, the newly designed sensor can be advantageously used in a wide range of applications, such as gas sensing, biosensing, and chemical sensing.

3.4 Conclusion

In this study, an optical fiber sensor for RI detection has been designed utilizing a configuration in which S-AuNW is implemented inside a fiber cladding hole. By allowing the analyte to be contained inside the hole in the proposed sensor, the effects of the environment are reduced and the analyte RI is determined with greater accuracy. In the context of this study, FEM has been used to simulate the sensor results and optimize its geometry parameters for better performance. The sensor obtains enhanced sensitivity by optimizing the separation between the curve boundary (B_s), the diameter of the hole (D_h), and the diameter of the S-AuNW (d_{Au}). These parameters play a crucial role in enhancing the sensor's ability to detect slight analyte RI changes, making it highly sensitive and applicable in various fields. The numerical simulation results showed that the SPR sensor, with S-AuNW assisted inside the hole in the fiber cladding, has achieved average sensitivity, maximum sensitivity, and FOM of 6700 nm/RIU, 14000 nm/RIU, and 124.54 RIU^{-1}, respectively. Additionally, the resolution of the designed sensor reached a maximum value of 7.14×10^{-6} within the 1.33-1.43 range of analyte RIs. my designed sensor has the capability to detect toxic and environmentally affected gases and chemicals as the analyte is placed inside the hole.